ACS APPLIED MATERIALS & INTERFACES

Research Article

Cite This: ACS Appl. Mater. Interfaces 2018, 10, 38928−38935

www.acsami.org

Dendrite Suppression Membranes for Rechargeable Zinc Batteries

Byoung-Sun Lee,[†] Shuang Cui,[‡] Xing Xing,[†] Haodong Liu,[†] Xiujun Yue,[†] Victoria Petrova,[†] Hee-Dae Lim,[†,§] Renkun Chen,[‡] and Ping Liu*[,†]

[†]Department of NanoEngineering and [‡]Department of Mechanical and Aerospace Engineering, University of California, San Diego, La Jolla, California 92093, United States

Supporting Information

ABSTRACT: Aqueous batteries with zinc metal anodes are promising alternatives to Li-ion batteries for grid storage because of their abundance and benefits in cost, safety, and nontoxicity. However, short cyclability due to zinc dendrite growth remains a major obstacle. Here, we report a cross-linked polyacrylonitrile (PAN)-based cation exchange membrane that is low cost and mechanically robust. Li_2S_3 reacts with PAN, simultaneously leading to cross-linking and formation of sulfur-containing functional groups. Hydrolysis of the membrane results in the formation of a membrane that achieves preferred cation transport and homogeneous ionic flux distribution. The separator is thin (30 μm-thick), almost 9 times stronger than hydrated Nafion, and made of low-cost materials. The membrane separator enables exceptionally long cyclability (>350 cycles) of Zn/Zn symmetric cells with low polarization and effective dendrite suppression. Our work demonstrates that the design of new separators is a fruitful pathway to enhancing the cyclability of aqueous batteries.

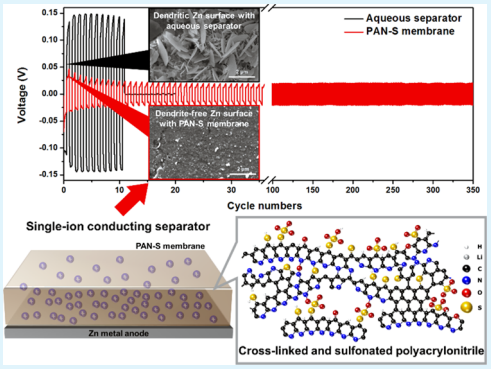

KEYWORDS: *aqueous battery separator, dendrite growth suppression, zinc battery, ion flux distribution, single-ion transport*

1. INTRODUCTION

Nonaqueous electrolyte-based Li-ion batteries are the overwhelming power source of choice for portable devices and electric vehicles because of their high energy density. The technology has more competition in grid-storage applications where various aqueous electrolyte-based systems are being actively pursued. Flow batteries, such as vanadium redox and all iron-based systems, are perceived to offer advantages in cost and safety.[1,2] Zn, which is nontoxic, inexpensive, and abundant,[3] has long been recognized as one of the most promising anode materials for aqueous batteries. Zn offers a high specific capacity of 820 mA h/g and low polarization.[4] The cathode chemistry can be versatile, including oxides of manganese, iron, and nickel as well as oxygen, however, rechargeability of these batteries has been limited. One of the major challenges is the dendrite formation on Zn electrode surface during charging. Strategies to suppress dendrite formation have mainly included electrolyte and electrode modifications through the use of electrolyte salts,[5] organic or inorganic additives,[1,6] and ionic liquid electrolytes.[7] Recently, three-dimensional Zn electrode structures have promised enhanced cyclability because of reduced effective current density.[4]

Membrane separator design is a promising option to suppress dendrite formation because the ion transport can be regulated by the separator. However, there have hardly been any studies on this topic. Zinc-based aqueous batteries have predominantly used few hundred microns thick glass fiber[6,8−10] or filter paper separators[5,11−13] because of low cost (e.g., 19 USD/m^2),[14] mechanical robustness, and limited resistance across the separator because of the high ionic conductivity of the aqueous electrolyte (up to 1 S/cm).[2] Meanwhile, gel polymer electrolytes using various water-soluble polymers [e.g., polyacrylic acid (PAA),[15] polyvinyl alcohol (PVA),[16] PVA−PAA,[17] and gelatin[18] have been employed as separators for enabling planar or cable-shaped flexible aqueous batteries because of their chemical stability and mechanical flexibility. A polymer-free gel electrolyte separator supported by a glass fiber mat containing salts (e.g., $ZnSO_4$ and Li_2SO_4) and gelling agents (e.g., fumed silica and β-cyclodextrin) was reported to suppress dendrites but with no significant cycling performance improvement.[19] Thus, the contribution of the separator to the improvement of cycling stability by suppressing dendrites remains unproven. An ion-exchange membrane might be highly advantageous as a battery separator to enhance the cycling stability of the zinc electrode. Two mechanisms can be operational: (i) a selective positive ion-conducting membrane can mitigate the ion concentration gradient, the primary source of dendrite growth and (ii) the intermolecular solvent channels in the membranes can greatly enhance the uniformity of current distribution resulting in a uniform zinc deposition.

Received: August 15, 2018
Accepted: October 23, 2018
Published: October 23, 2018

Downloaded via UNIV OF CALIFORNIA SAN DIEGO on March 19, 2019 at 20:49:54 (UTC).
See https://pubs.acs.org/sharingguidelines for options on how to legitimately share published articles.

© 2018 American Chemical Society

DOI: 10.1021/acsami.8b14022
ACS Appl. Mater. Interfaces 2018, 10, 38928−38935

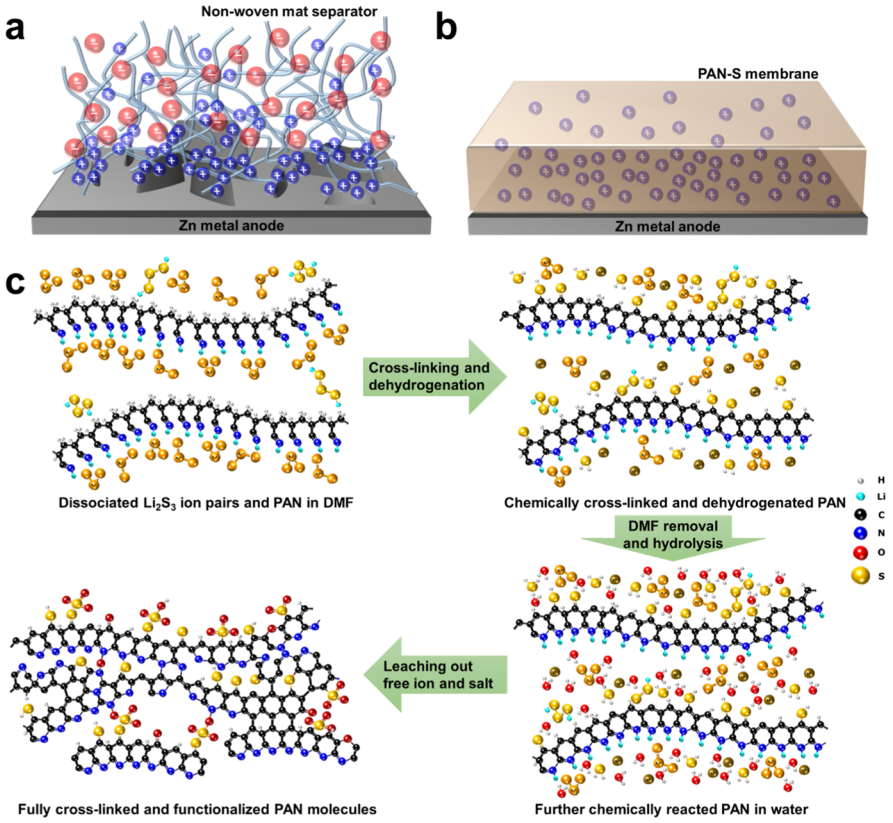

Figure 1. Schematic descriptions of Zn deposition: (a) Zn dendritic growth due to the ramified Zn deposition at the interface between the Zn metal and conventional separator and (b) dendrite growth suppression due to uniform Zn^{2+} concentration at the interface between the Zn metal and the single-ion transport membrane. (c) Proposed synthesis route for the novel PAN-S membrane.

In fact, nonporous cationic exchange membranes, such as Nafion, have been investigated as a single-ion conducting polymer electrolyte and separator to suppress the dendrite formation of Li in nonaqueous batteries.[20,21] Its use in aqueous batteries has been challenging. It is prohibitively expensive, about 1200 USD/m^2[22,22] versus 2 USD/m^2 for microporous battery separators for electric vehicles.[23] Moreover, commercial Nafion membranes are thick (e.g., 210 μm for Nafion 117) because the mechanical properties of the hydrated Nafion membrane is rather poor, with a Young's modulus of ~114 MPa for Nafion 117.[24] Therefore, it is necessary to develop a low cost, mechanically robust ionic conducting membrane to serve as the aqueous battery separator, which can suppress dendrite formation without sacrificing the energy density. In this work, a low cost and mechanically robust polyacrylonitrile (PAN)-based cationic exchange membrane is described. PAN is cross-linked with a polysulfide compound, which contributes sulfonate groups. PAN also has the benefits of being low cost (4.4−13.2 USD/kg)[25] and readily cross-linkable.[26,27] We present the synthesis, structural characterization, and performance evaluation of the membrane in zinc electrode-based cells to demonstrate its ability of suppressing dendrites.

2. EXPERIMENTAL SECTION

2.1. Materials. The solutes [e.g., PAN (M_w = 150 000 g mol^{-1}), Li_2S, and elemental sulfur (S8)] were purchased from Sigma-Aldrich, whereas *N*,*N*-dimethylformamide (DMF, ≥ 99.8%) was supplied by Fisher Scientific. All chemicals were used without purification.

2.2. Fabrication. Synthesis of the membrane precursor followed the previous work by Guo et al.[28] Sulfur (0.64 g) and 0.46 g of Li_2S were dissolved in 4.72 g of DMF to make the stoichiometry of Li_2S_3 in the solution, while 0.53 g of PAN was dissolved in 4.72 g of DMF. The solutions were stirred overnight at room temperature. After the solutes fully dissolved in the solvent, 1.94 g of Li_2S_3 solution and 1.76 g of PAN solution were vigorously mixed and subsequently screen-printed on a glass slide with a doctor blade (gap width: 500 μm). The coated solution was stored in an Ar-filled glovebox for 5 days to allow Li_2S_3 and PAN to react and dry. The solidified film was then heated at 100 °C for 4 h in an ambient atmosphere to finish the cross-linking and further dried at 100 °C overnight under vacuum to remove the residual solvents. Because the dried film contains nonchemically bonded lithium polysulfide salts, the film was further treated in boiling water for 1 h multiple times to leach out the free salts, until the salts were fully removed. The process is schematically shown in Figure S1.

2.3. Characterization. The molecular structure was carefully examined by employing X-ray photoelectron spectroscopy (XPS, Kratos Analytical, Kratos AXIS Supra) and Fourier transform infrared spectroscopy (FT-IR, PerkinElmer, Spectrum 100 FT-IR).

Various baseline material properties of the hydrated membrane were also evaluated. Mechanical behavior was assessed using the tensile test (5960 universal testing system, Instron), and water uptake and thermal stability were examined using thermogravimetric analysis (TGA, Pyris 1 TGA, PerkinElmer).

Morphologies of the prepared membrane were investigated using scanning electron microscopy (SEM, FEI Quanta FEG 250) and atomic force microscopy (AFM, Nanoscope V multimode AFM, Bruker), and crystallographic characterization was conducted using wide-angle X-ray diffraction (XRD, Bruker, D2 Phaser 2nd generation). The electrochemical properties were examined using electrochemical impedance spectroscopy (EIS) and chronoamperometry using a potentiostat (Gamry Interface 1000).

2.4. Zn/Zn Symmetric Cycling Test. To test as a separator, the membrane was assembled into the 2032-type coin cell in between two Zn foil disks (620 μm thick, Alfa Aesar) with one spring and two spacers (500 μm thick, MTI). A commercial nonwoven separator for

DOI: 10.1021/acsami.8b14022
ACS Appl. Mater. Interfaces 2018, 10, 38928−38935

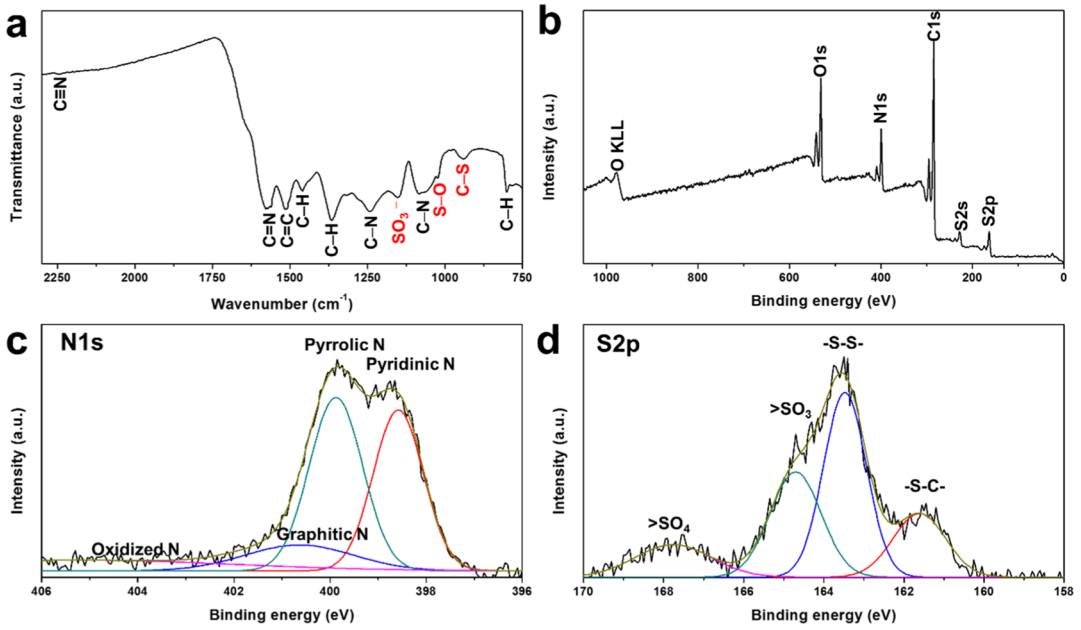

Figure 2. Molecular structural characterization results of the stabilized PAN-S membrane: (a) FT-IR spectra, (b) survey scan spectra of XPS, and (c,d) high-resolution XPS spectra of (c) N 1s and (d) S 2p.

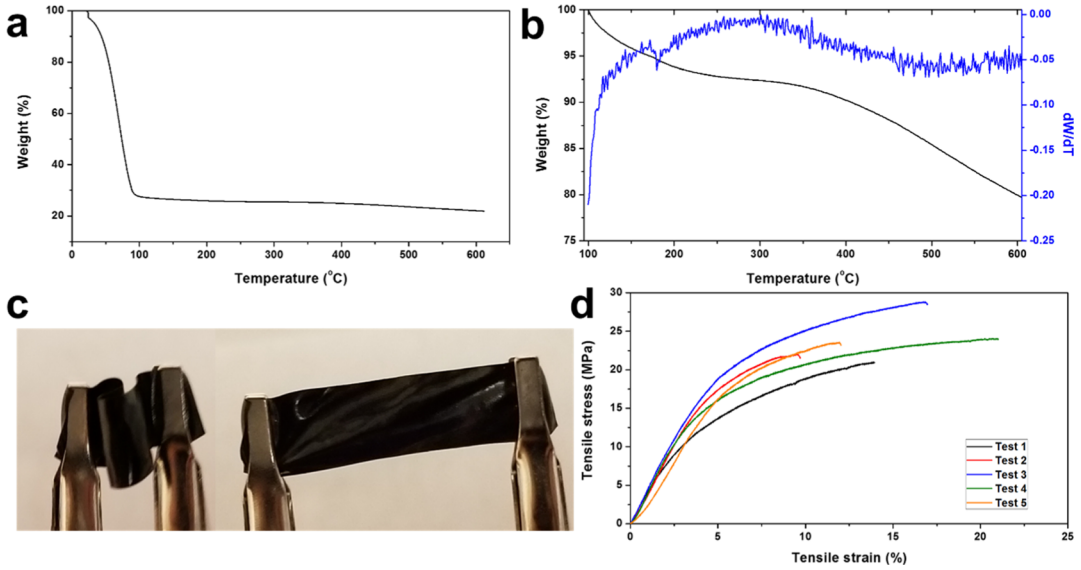

Figure 3. Thermal and mechanical properties of PAN-based ionic exchange hydrated membrane: (a) TGA profile in a wide temperature range showing the high water content loss at below 100 °C; (b) TGA profile highlighting the weight loss at above 100 °C; (c) photographs of bent and stretched PAN-S film; and (d) stress–strain curves for five repeated runs.

aqueous batteries (FS 22145-14 E, Freudenberg) was used as a reference. $ZnSO_4$ aqueous solution (2 M) was employed as the electrolyte. Galvanostatic cycling was performed at a constant current density of 0.5 mA/cm^2 for 30 min during each charge and discharge step. Zn anode surface morphologies after the first discharge and half-charge cycles were observed under SEM.

3. RESULTS AND DISCUSSION

On the basis of studies on Li dendrite formation in nonaqueous electrolytes, the major causes of dendrite growth on a metal anode are unstable ion transport, mechanically weak electrolyte, and unregulated surface reaction.[29] Likewise, zinc anodes are highly vulnerable to dendrite growth when glass fiber or filter paper separators are employed because the nonselective ion transport through the separator results in concentration gradients close to the Zn anode, and there is no physical barrier to suppress the dendrite growth, as described in Figure 1a. In contrast, a nonporous gel polymer electrolyte can result in dendrite suppression because of single-ion transport and uniform ionic flux distribution, as shown in Figure 1b.

The synthesis of PAN-based ionic conducting membrane (PAN-S membrane) is schematically shown in Figure 1c. PAN was employed to form a mechanically robust skeleton, and lithium polysulfide (Li_2S_3) was used for two reasons: (i) promoting chemical cross-linking reactions of PAN and (ii) providing sulfur atoms to endow sulfonyl functional groups. Note that lithium polysulfide-induced cross-linking of PAN has been reported before with the resulting material used as a

DOI: 10.1021/acsami.8b14022
ACS Appl. Mater. Interfaces 2018, 10, 38928–38935

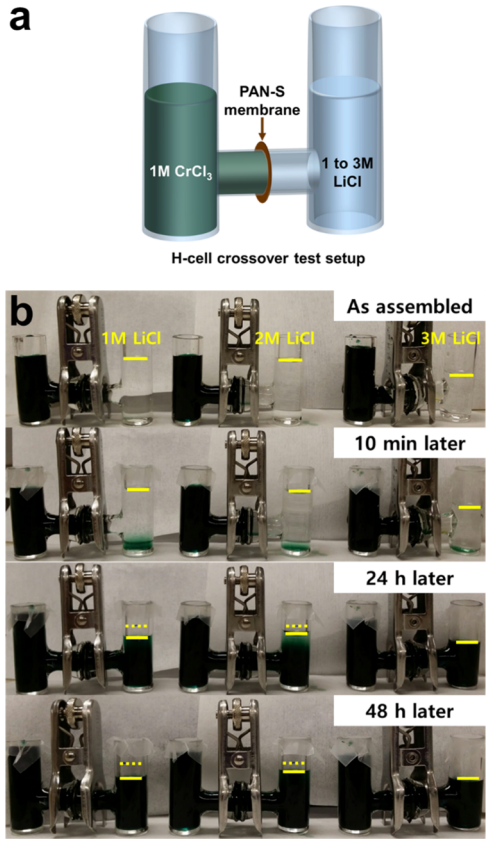

Figure 4. Ionic transport properties: (a) schematic diagram of cross-over testing H-cell setup and (b) 1 M $CrCl_3$–x M LiCl cross-over test (x = 1, 2, and 3) results up to 48 h.

battery cathode in a nonaqueous electrolyte.[28] Here, PAN reacts with Li_2S_3 in a cast film and is subsequently allowed to react with water to form a hydrous membrane. The detailed procedures are schematically described in Figure S1. The cross-linking reaction of PAN, which is also known as stabilization or cyclization,[26] proceeds by transformation of the triple bonds of the nitrile group (−C≡N) into −C═N double and −C−N single bonds in the presence of dissolved Li_2S_3 in DMF. FT-IR spectra of the unhydrolyzed Li_2S_3−PAN membrane in Figure S2 reveals significantly reduced −C≡N peaks at around 2240 cm^{-1}, and −C═N double and −C−N single bonds increased at around 1578 and 1240 cm^{-1}, respectively, in comparison to raw PAN.[30−32] After hydrolysis, the nitrile group (−C≡N) peak completely disappeared and C−H peaks (e.g., at around 2950 and 1455 cm^{-1}) were significantly reduced, which indicates that further cross-linking reactions including dehydrogenation took place during the boiling process in distilled water, as shown in Figure S2.[33,34] The time and duration of the hydrolysis were systematically investigated. Figure S3 shows the molecular structure as measured by FT-IR, and the ionic conductivity of the membrane stabilized after a repeated boiling process. FT-IR spectra in Figure 2a show that the cross-linked molecules consist of partially dehydrogenated aromatic rings containing nitrogen and functionalized with sulfonate ions after the repeated boiling process based on the following peak information: aromatic C═C bond at 1517−1508 cm^{-1}, −C═N double bond at 1578 cm^{-1},−C−N single bond at 1240 and 1083 cm^{-1}, C−H bond at 1455, 1365, and 800 cm^{-1}, and sulfonate ion-related bonds at 1152 (SO_3^- bonded to aromatic ring), 1024 (S−O), and 940 cm^{-1} (C−S).[32,35−38]

A 30 μm-thick film was prepared, which consists of carbon, nitrogen, sulfur, and oxygen, as shown by energy dispersive X-ray spectroscopy (EDX) results presented in Figure S4. Because lithium cannot be detected by EDX, XPS was employed. XPS survey spectra in Figure 2b reveal that the prepared membrane consists of carbon, nitrogen, sulfur, and oxygen, and the lithium salt was fully removed by the repeated boiling process because of a lack of signal at 55 eV.[36] N 1s XPS spectra in Figure 2c show that the nitrogen atoms are mainly involved in the aromatic ring structures such as pyridine (398.6 eV) and pyridone (and/or pyrrole, 399.9 eV) structures, whereas the portions of the oxidized nitrogen (405.2 eV) or the nitrogen atoms placed at the graphitic (or quaternary) position (400.6 eV) are not significant.[39,40] S 2p XPS spectra in Figure 2d exhibited four peaks: a peak at 161.6 eV attributed to sulfide (S^{2-}) from thioketone (C═S),[41] two peaks at 163.5 and 164.7 eV related to $2p_{3/2}$ and $2p_{1/2}$ positions of the −C−S− covalent bond,[42] and a broad peak at 167.8 eV that originated from $-SO_3^-$.[43] In brief, the molecular structure of the PAN-S membrane was built with cross-linked PAN functionalized with the sulfonate group, as shown in Figure 1c.

As the PAN-S membrane was functionalized with the ionic functional groups (e.g., $-SO_3^-$), the membrane is not only ionically conducting (8.12×10^{-5} S/cm from the high-frequency Z_{Re} intercept of EIS spectra in Figure S5a) but also readily hydrated under room temperature because of its hygroscopic characteristics.[44] TGA was conducted to quantify the hydrolysis and thermal stability of the PAN-S membrane. Full range TGA spectra in Figure 3a reveal a significant weight loss (72.4%) as the temperature increased to 100 °C because of high water contents. Figure 3b shows the thermal stability of the membrane because of the cross-linked molecular structure, with the weight loss by desulfonation taking place between 170 and 300 °C[45,46] and thermal decomposition of cross-linked PAN molecules at above 300 °C.[47] Thus, the cross-linked PAN backbone provides thermal stability, whereas the high water content in the membrane is attributed to the sulfone functional group. The high water contents enable the uptake of additional zinc salts after being soaked in the zinc electrolyte (2 M $ZnSO_4$ solution) (see Figure S5b), leading to a high ionic conductivity (3.32×10^{-3} S/cm at room temperature). This conductivity is comparable to the previous polymer gel electrolytes for the zinc batteries (ca. 10^{-3} S/cm at room temperature).[48,49]

Photographs in Figure 3c reveal that the PAN-S membrane has a black color and can be folded and stretched. The black color of the membrane is attributed to the cross-linking reaction.[26] Despite its highly hygroscopic characteristic,[44] the hydrated membrane is very strong. Mechanical properties of the hydrated PAN-S membrane were measured using the tensile test, as shown in Figure 3d, and are summarized in Table S1. The average Young's modulus and strength of the membrane were 391.1 MPa (±58.9 MPa) and 23.62 MPa (±2.99 MPa), respectively, whereas the average elongation at break was 14.73% (±4.41%). The Young's modulus of the membrane is almost 9 times higher than that of the wet Nafion membrane (43.8 MPa), whereas the strength is comparable to that of the wet Nafion (20.88 MPa) (refer to Figure S6). The high Young's modulus allows a reduction in thickness when used as a separator while still holding large amounts of electrolyte.

DOI: 10.1021/acsami.8b14022
ACS Appl. Mater. Interfaces 2018, 10, 38928−38935

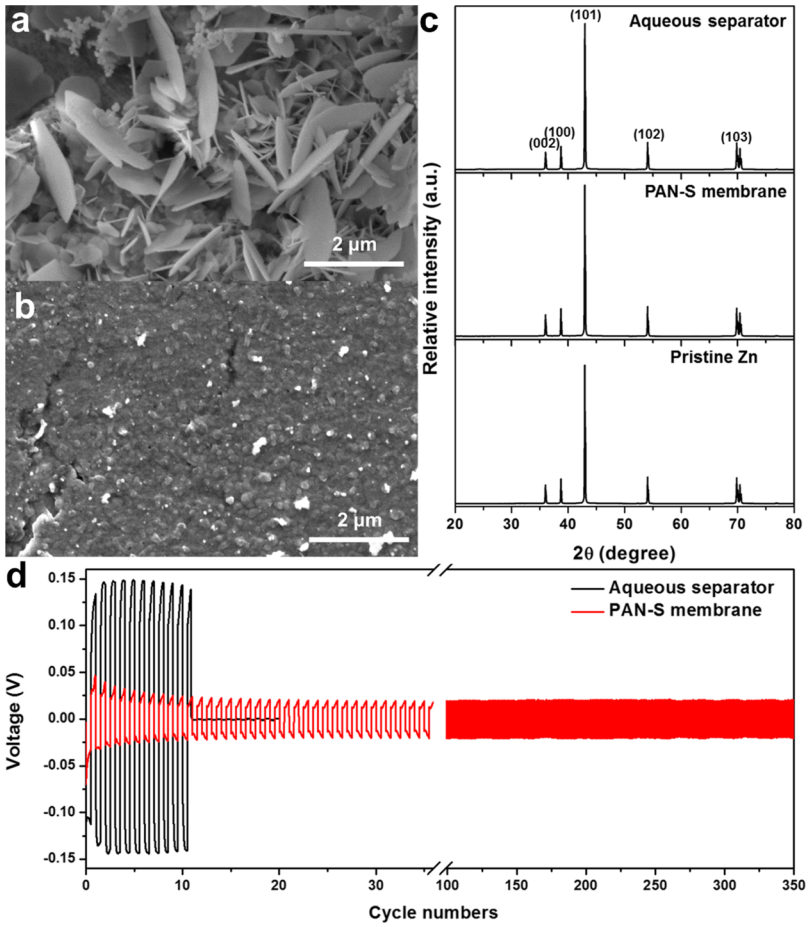

Figure 5. Zn/Zn symmetric cell test results at a current density of 0.5 mA/cm^2. Morphological and crystallographic characterizations of the 30 min-stripped and 15 min-deposited Zn anode: SEM images of the Zn anode surface from the cells using a (a) aqueous separator and (b) PAN-S membrane. (c) Identical XRD patterns of pristine and deposited Zn. (d) Cycling performance comparison.

When used as a separator, the pin-hole free PAN-S membrane (Figure S7) was expected to be better than conventional separators with regard to dendrite suppression for the following two reasons: (i) better ionic flux distribution through the large number of nanosized water domains and (ii) selective cationic transport due to the ionic functional groups (e.g., $-SO_3^-$). The water domain formed in the PAN-S membrane was identified as the dark region in AFM images, and the measured domain sizes from small-angle X-ray scattering ranged from 123.2 to 18.4 nm (refer to Figure S8). Thus, Zn^{2+} ions transport along the connected hydrophilic channels formed by the ionic clusters of the hydrated PAN-S membrane (Figure S9).[50] Cross-over tests were conducted to demonstrate the selective ion transport, as shown in Figure 4. $CrCl_3$ solution (5 mL, 1 M) was added at the left-hand side of the membrane, while an equal amount of 1−3 M LiCl solution was added at the right-hand side of membrane. With 1 M LiCl, both sides have equal moles of cations. LiCl (2 M) versus 1 M $CrCl_3$ have the same moles of total ions. Finally, 3 M LiCl provides a total anion balance. Note that the dotted and solid yellow lines represent the original and final levels of the LiCl solutions. The LiCl solutions turned a faint green color after 10 min and a deep green color after 48 h because of Cr^{3+} cation migration. On the other hand, the lowered levels of 1 M and 2 M LiCl solutions were attributed to the osmotic drag for balancing the anion concentration. $CrCl_3$ (1 M)−1 M $ZnCl_2$ cross-over test was further conducted to directly examine the selective transport of the cation and immobilization of the anion (Figure S10). Results from a Nafion membrane were included for comparison. The level of 1 M $ZnCl_2$ solution was lowered after 24 h for both membranes because of the osmotic drag for balancing the anion concentration. The PAN-S membrane behavior in this test is exactly the same phenomenon with the 1 M $CrCl_3$−x M LiCl cross-over test results (x = 1 and 2). Thus, it could be concluded that the PAN-S membrane selectively and effectively transports the cation and immobilizes the anion.

The performance of the membrane in a zinc-based battery is first evaluated by observing the morphology of Zn deposits under galvanostatic conditions in a Zn/Zn cell. The current density is 0.5 mA/cm^2, and the electrolyte is a 2 M $ZnSO_4$ aqueous solution. The dendrite growth on the electrode was examined after stripping for 30 min and plating at the same current density for 15 min to cycle the freshly plated zinc (refer Figure S11). The profile is chosen to show the early stage growth of zinc on a "fresh" surface created by stripping first, and the difference is already dramatic. Flower-shaped dendrites were observed when the conventional aqueous separator was used as shown in Figure 5a, which was attributed to nonuniform Zn^{2+} ion flux due to the large pores in the separator, as described in Figure 1a.[51,52] On the other hand, a dendrite-free surface was observed in Figure 5b when the PAN-S membrane was used as the separator because the flux of the cation was uniformly distributed by the membrane as

DOI: 10.1021/acsami.8b14022
ACS Appl. Mater. Interfaces 2018, 10, 38928−38935

shown in Figure 1b. Moreover, ion selectivity of the separator helped to mitigate the concentration gradients by limiting the anion mobility.[53]

Finally, cycling performances of the Zn/Zn symmetric cells were examined (Figure 5d). Voltage−time profiles of the Zn/aqueous separator/Zn cell showed typical behavior with a high voltage hysteresis (~280 mV) and the cell short-circuited at the 11th cycle. In contrast, the voltage−time profile of the Zn/PAN-S membrane/Zn showed stable cycling with a low voltage hysteresis of <40 mV through 350 cycles. The smaller polarization observed for the cell with the PAN-S membrane is possibly due to the lower overpotential for zinc nucleation because the nonwoven aqueous separator is expected to have a lower ionic resistance. The PAN-S membrane has a selectivity for cation transport and is mechanically compliant, both of which would promote uniform ion flux and zinc nucleation. Similar observations have been made in lithium metal systems,[54] but the exact cause for zinc requires further investigation. Longer time (2 h) stripping/plating test under the same current density (0.5 mA/cm^2) at the charge amount of 1 mA h/cm^2 was conducted to demonstrate the advantage of the PAN-S membrane (Figure S12). It is noteworthy that the aqueous separator-based cell was short-circuited right after 1 h stripping, whereas the PAN-S membrane-based cell stably cycled under the same condition. In addition, stripping/plating tests for the PAN-S membrane under increased current densities (1 and 2 mA/cm^2) and capacities of 0.5 and 1 mA h/cm^2 were conducted (Figure S13). Despite the slightly increased voltage hysteresis (ca. 53 and 65 mV) as the current density increased, the PAN-S membrane-based cells stably cycled for more than 50 cycles because of effective dendrite suppression. Therefore, we concluded that zinc dendrite formation in an aqueous electrolyte was effectively suppressed and cyclability was significantly improved by the cationic exchange membrane because of the uniform ionic flux distribution and cation selectivity.

4. CONCLUSIONS

A low cost and mechanically robust membrane was synthesized by cross-linking PAN with lithium polysulfide followed by hydrolysis. The cross-linked molecular structure provides mechanical robustness with a high Young's modulus of 391.1 MPa and thermal stability, whereas the hygroscopic and cationic selective transport characteristics were enabled by the sulfonic functional group. When used as the separator in a Zn/Zn battery cell, excellent electrochemical performances such as suppressed dendrite formation, small polarization (<40 mV), and long cycling stability of 350 cycles were observed. This performance enhancement is likely due to the even ion flux distribution and preference of the membrane to transport cations, which reduces the concentration gradient. The membrane is thin, robust, and made of inexpensive commodity materials and represents a new solution for rechargeable aqueous battery separators. More work is needed to evaluate the membrane with promising cathode materials such as manganese oxide and oxygen.[55] We expect our low-cost separator to contribute to the advancement of technology, leading to low-cost, long-life solutions for grid storage.

■ ASSOCIATED CONTENT

Supporting Information

The Supporting Information is available free of charge on the ACS Publications website at DOI: 10.1021/acsami.8b14022.

Supplementary structural and morphological characterization data (PDF)

■ AUTHOR INFORMATION

Corresponding Author

*E-mail: piliu@eng.ucsd.edu.

ORCID

Renkun Chen: 0000-0001-7526-4981

Ping Liu: 0000-0002-1488-1668

Present Address

§(H.-D.L.) Center for Energy Convergence Research, Green City Technology Institute, Korea Institute of Science and Technology, Seoul, 02792, Republic of Korea.

Notes

The authors declare no competing financial interest.

■ ACKNOWLEDGMENTS

This work was supported by the Advanced Research Projects Agency-Energy, US Department of Energy, under contract no. DE-AR0000781. This work was performed in part at the San Diego Nanotechnology Infrastructure of UCSD, a member of the National Nanotechnology Coordinated Infrastructure, which is supported by the National Science Foundation (grant ECCS-1542148).

■ REFERENCES

(1) Sun, K. E. K.; Hoang, T. K. A.; Doan, T. N. L.; Yu, Y.; Zhu, X.; Tian, Y.; Chen, P. Suppression of Dendrite Formation and Corrosion on Zinc Anode of Secondary Aqueous Batteries. *ACS Appl. Mater. Interfaces* **2017**, *9*, 9681−9687.

(2) Kundu, D.; Adams, B. D.; Duffort, V.; Vajargah, S. H.; Nazar, L. F. A High-Capacity and Long-Life Aqueous Rechargeable Zinc Battery Using a Metal Oxide Intercalation Cathode. *Nat. Energy* **2016**, *1*, 16119.

(3) Xu, C.; Li, B.; Du, H.; Kang, F. Energetic Zinc Ion Chemistry: The Rechargeable Zinc Ion Battery. *Angew. Chem., Int. Ed.* **2012**, *51*, 933−935.

(4) Parker, J. F.; Chervin, C. N.; Pala, I. R.; Machler, M.; Burz, M. F.; Long, J. W.; Rolison, D. R. Rechargeable Nickel-3D Zinc Batteries: An Energy-dense, Safer Alternative to Lithium-ion. *Science* **2017**, *356*, 415−418.

(5) Zhang, N.; Cheng, F.; Liu, Y.; Zhao, Q.; Lei, K.; Chen, C.; Liu, X.; Chen, J. Cation-Deficient Spinel $ZnMn_2O_4$ Cathode in Zn-$(CF_3SO_3)_2$ Electrolyte for Rechargeable Aqueous Zn-Ion Battery. *J. Am. Chem. Soc.* **2016**, *138*, 12894−12901.

(6) Pan, H.; Shao, Y.; Yan, P.; Cheng, Y.; Han, K. S.; Nie, Z.; Wang, C.; Yang, J.; Li, X.; Bhattacharya, P.; Mueller, K. T.; Liu, J. Reversible Aqueous Zinc/Manganese Oxide Energy Storage from Conversion Reactions. *Nat. Energy* **2016**, *1*, 16039.

(7) Liu, Z.; Pulletikurthi, G.; Lahiri, A.; Cui, T.; Endres, F. Suppressing the Dendritic Growth of Zinc in an Ionic Liquid Containing Cationic and Anionic Zinc Complexes for Battery Applications. *Dalton Trans.* **2016**, *45*, 8089−8098.

(8) Wu, X.; Li, Y.; Xiang, Y.; Liu, Z.; He, Z.; Wu, X.; Li, Y.; Xiong, L.; Li, C.; Chen, J. The Electrochemical Performance of Aqueous Rechargeable Battery of Zn/$Na_{0.44}MnO_2$ Based on Hybrid Electrolyte. *J. Power Sources* **2016**, *336*, 35−39.

(9) Yesibolati, N.; Umirov, N.; Koishybay, A.; Omarova, M.; Kurmanbayeva, I.; Zhang, Y.; Zhao, Y.; Bakenov, Z. High Performance Zn/$LiFePO_4$ Aqueous Rechargeable Battery for Large Scale Applications. *Electrochim. Acta* **2015**, *152*, 505−511.

(10) Lu, C.; Hoang, T. K. A.; Doan, T. N. L.; Zhao, H.; Pan, R.; Yang, L.; Guan, W.; Chen, P. Rechargeable Hybrid Aqueous Batteries Using Silica Nanoparticle Doped Aqueous Electrolytes. *Appl. Energy* **2016**, *170*, 58−64.

(11) Minakshi, M.; Ionescu, M. Anodic Behavior of Zinc in Zn-MnO_2 Battery Using ERDA Technique. *Int. J. Hydrogen Energy* **2010**, *35*, 7618−7622.
(12) Minakshi, M.; Singh, P.; Appadoo, D.; Martin, D. E. Synthesis and Characterization of Olivine $LiNiPO_4$ for Aqueous Rechargeable Battery. *Electrochim. Acta* **2011**, *56*, 4356−4360.
(13) Kandhasamy, S.; Pandey, A.; Minakshi, M. Polyvinylpyrrolidone Assisted Sol−Gel Route $LiCo_{1/3}Mn_{1/3}Ni_{1/3}PO_4$ Composite Cathode for Aqueous Rechargeable Battery. *Electrochim. Acta* **2012**, *60*, 170−176.
(14) Li, H. *Qualitative Blood Coagulation Test Using Paper-Based Microfluidic Lateral Flow Device*; University of Cincinnati, 2014, p 19.
(15) Gaikwad, A. M.; Whiting, G. L.; Steingart, D. A.; Arias, A. C. Highly Flexible, Printed Alkaline Batteries Based on Mesh-Embedded Electrodes. *Adv. Mater.* **2011**, *23*, 3251−3255.
(16) Liu, J.; Guan, C.; Zhou, C.; Fan, Z.; Ke, Q.; Zhang, G.; Liu, C.; Wang, J. A Flexible Quasi-Solid-State Nickel-Zinc Battery with High Energy and Power Densities Based on 3D Electrode Design. *Adv. Mater.* **2016**, *28*, 8732−8739.
(17) Wang, Z.; Wu, Z.; Bramnik, N.; Mitra, S. Fabrication of High-Performance Flexible Alkaline Batteries by Implementing Multiwalled Carbon Nanotubes and Copolymer Separator. *Adv. Mater.* **2014**, *26*, 970−976.
(18) Park, J.; Park, M.; Nam, G.; Lee, J.-s.; Cho, J. All-Solid-State Cable-Type Flexible Zinc-Air Battery. *Adv. Mater.* **2015**, *27*, 1396−1401.
(19) Hoang, T. K. A.; Doan, T. N. L.; Lu, C.; Ghaznavi, M.; Zhao, H.; Chen, P. Performance of Thixotropic Gel Electrolytes in the Rechargeable Aqueous Zn/$LiMn_2O_4$ Battery. *ACS Sustain. Chem. Eng.* **2017**, *5*, 1804−1811.
(20) Lu, Y.; Tikekar, M.; Mohanty, R.; Hendrickson, K.; Ma, L.; Archer, L. A. Stable Cycling of Lithium Metal Batteries Using High Transference Number Electrolytes. *Adv. Energy Mater.* **2015**, *5*, 1402073.
(21) Song, J.; Lee, H.; Choo, M.-J.; Park, J.-K.; Kim, H.-T. Ionomer-Liquid Electrolyte Hybrid Ionic Conductor for High Cycling Stability of Lithium Metal Electrodes. *Sci. Rep.* **2015**, *5*, 14458.
(22) Javakhishvili, I.; Dimitrov, I.; Tynelius, O.; Hales, J.; Jankova, K.; Hvilsted, S. Surface-Initiated Atom Transfer Radical Polymerization from Electrospun Mats: An Alternative to Nafion. *Macromol. Mater. Eng.* **2017**, *302*, 1600410.
(23) Carlson, S. *Innovative Manufacturing and Materials for Low Cost Lithium Ion Batteries*, DOE-OPTO-05433-1; Optodot Corporation: Woburn, MA (United States), 2015; pp 1−31.
(24) He, S. S.; Strickler, A. L.; Frank, C. W. A Semi-Interpenetrating Network Approach for Dimensionally Stabilizing Highly-Charged Anion Exchange Membranes for Alkaline Fuel Cells. *ChemSusChem* **2015**, *8*, 1472−1483.
(25) Baker, D. A.; Rials, T. G. Recent Advances in Low-Cost Carbon Fiber Manufacture from Lignin. *J. Appl. Polym. Sci.* **2013**, *130*, 713−728.
(26) Bashir, Z. A Critical Review of the Stabilisation of Polyacrylonitrile. *Carbon* **1991**, *29*, 1081−1090.
(27) Mathur, R. B.; Bahl, O. P.; Mittal, J.; Nagpal, K. C. Structure of Thermally Stabilized PAN Fibers. *Carbon* **1991**, *29*, 1059−1061.
(28) Guo, J.; Yang, Z.; Yu, Y.; Abruña, H. D.; Archer, L. A. Lithium-Sulfur Battery Cathode Enabled by Lithium-Nitrile Interaction. *J. Am. Chem. Soc.* **2013**, *135*, 763−767.
(29) Tikekar, M. D.; Choudhury, S.; Tu, Z.; Archer, L. A. Design Principles for Electrolytes and Interfaces for Stable Lithium-Metal Batteries. *Nat. Energy* **2016**, *1*, 16114.
(30) Yue, Z.; Benak, K. R.; Wang, J.; Mangun, C. L.; Economy, J. Elucidating the Porous and Chemical Structures of $ZnCl_2$-Activated Polyacrylonitrile on a Fiberglass Substrate. *J. Mater. Chem.* **2005**, *15*, 3142−3148.
(31) Qiao, H.; Fei, Y.; Chen, K.; Cui, R.; Wei, Q. Electrospun Synthesis and Electrochemical Property of Zinc Ferrite Nanofibers. *Ionics* **2016**, *22*, 967−974.
(32) Shen, L.; Shen, L.; Wang, Z.; Chen, L. In Situ Thermally Cross-linked Polyacrylonitrile as Binder for High-Performance Silicon as Lithium Ion Battery Anode. *ChemSusChem* **2014**, *7*, 1951−1956.
(33) Deniau, G.; Viel, P.; Valin, F.; Lécayon, G.; Pirlot, C.; Bertholet, J. C.; Demortier, G.; Delhalle, J. Analysis of the Chemical Transformations Induced at the Surface of Polyacrylonitrile and Polymethacrylonitrile Films by 5 keV Proton Beams. *Nucl. Instrum. Methods Phys. Res., Sect. B* **1999**, *151*, 109−117.
(34) Lee, B.-S.; Park, K.-M.; Yu, W.-R.; Youk, J. H. An Effective Method for Manufacturing Hollow Carbon Nanofibers and Microstructural Analysis. *Macromol. Res.* **2012**, *20*, 605−613.
(35) Bode-Aluko, C. A.; Pereao, O.; Fatoba, O.; Petrik, L. Surface-Modified Polyacrylonitrile Nanofibres as Supports. *Polym. Bull.* **2017**, *74*, 2431−2442.
(36) Kim, J.-S.; Hwang, T. H.; Kim, B. G.; Min, J.; Choi, J. W. A Lithium-Sulfur Battery with a High Areal Energy Density. *Adv. Funct. Mater.* **2014**, *24*, 5359−5367.
(37) Klaysom, C.; Ladewig, B. P.; Lu, G. Q. M.; Wang, L. Preparation and Characterization of Sulfonated Polyethersulfone for Cation-Exchange Membranes. *J. Membr. Sci.* **2011**, *368*, 48−53.
(38) Reddy, A. V. R.; Mohan, D. J.; Bhattacharya, A.; Shah, V. J.; Ghosh, P. K. Surface Modification of Ultrafiltration Membranes by Preadsorption of a Negatively Charged Polymer. *J. Membr. Sci.* **2003**, *214*, 211−221.
(39) Tran, M.-H.; Yang, C.-S.; Yang, S.; Kim, I.-J.; Jeong, H. K. Size Dependent Electrochemical Properties of Reduced Graphite Oxide. *Chem. Phys. Lett.* **2014**, *608*, 207−212.
(40) Lee, M.-S.; Park, M.; Kim, H. Y.; Park, S.-J. Effects of Microporosity and Surface Chemistry on Separation Performances of N-Containing Pitch-Based Activated Carbons for CO_2/N_2 Binary Mixture. *Sci. Rep.* **2016**, *6*, 23224.
(41) Zeng, Q. R.; Li, Y.; Wu, K.-H.; Huang, N.; Dalapati, S.; Su, B.-J.; Jang, L.-Y.; Gentle, I. R.; Jiang, D.; Wang, D.-W. Long-Chain Solid Organic Polysulfide Cathode for High-Capacity Secondary Lithium Batteries. *Energy Storage Mater.* **2018**, *12*, 30−36.
(42) Sun, D.; Ban, R.; Zhang, P.-H.; Wu, G.-H.; Zhang, J.-R.; Zhu, J.-J. Hair Fiber as a Precursor for Synthesizing of Sulfur- and Nitrogen-Co-Doped Carbon Dots with Tunable Luminescence Properties. *Carbon* **2013**, *64*, 424−434.
(43) Sun, C.; Zhang, Y.; Wang, P.; Yang, Y.; Wang, Y.; Xu, J.; Wang, Y.; Yu, W. W. Synthesis of Nitrogen and Sulfur Co-Doped Carbon Dots from Garlic for Selective Detection of Fe^{3+}. *Nanoscale Res. Lett.* **2016**, *11*, 110.
(44) Im, S. J.; Patel, R.; Shin, S. J.; Kim, J. H.; Min, B. R. Sulfonated Poly(Arylene Ether Sulfone) Membranes Based on Biphenol for Direct Methanol Fuel Cells. *Korean J. Chem. Eng.* **2008**, *25*, 732−737.
(45) Huang, C.-H.; Wu, H.-M.; Chen, C.-C.; Wang, C.-W.; Kuo, P.-L. Preparation, Characterization and Methanol Permeability of Proton Conducting Membranes Based on Sulfonated Ethylene-Vinyl Alcohol Copolymer. *J. Membr. Sci.* **2010**, *353*, 1−9.
(46) Sahu, A.; Selvarani, G.; Bhat, S.; Pitchumani, S.; Sridhar, P.; Shukla, A.; Narayanan, N.; Banerjee, A.; Chandrakumar, N. Effect of Varying Poly(styrene sulfonic acid) Content in Poly(vinyl alcohol)-Poly(styrene sulfonic acid) Blend Membrane and its Ramification in Hydrogen-oxygen Polymer Electrolyte Fuel Cells. *J. Membr. Sci.* **2008**, *319*, 298−305.
(47) Li, S.; Qin, X.; Zhang, H.; Wu, J.; He, Y.-B.; Li, B.; Kang, F. Silicon/Carbon Composite Microspheres with Hierarchical Core-shell Structure as Anode for Lithium Ion Batteries. *Electrochem. Commun.* **2014**, *49*, 98−102.
(48) Zhang, G.; Zhang, X. G. A Novel Alkaline Zn/MnO_2 Cell with Alkaline Solid Polymer Electrolyte. *Solid State Ionics* **2003**, *160*, 155−159.
(49) Xu, J. J.; Ye, H.; Huang, J. Novel Zinc Ion Conducting Polymer Gel Electrolytes Based on Ionic Liquids. *Electrochem. Commun.* **2005**, *7*, 1309−1317.
(50) Bakangura, E.; Wu, L.; Ge, L.; Yang, Z.; Xu, T. Mixed Matrix Proton Exchange Membranes for Fuel Cells: State of the Art and Perspectives. *Prog. Polym. Sci.* **2016**, *57*, 103−152.

DOI: 10.1021/acsami.8b14022
ACS Appl. Mater. Interfaces 2018, 10, 38928−38935

(51) Tan, J.; Ryan, E. M. Computational Study of Electro-Convection Effects on Dendrite Growth in Batteries. *J. Power Sources* **2016**, *323*, 67−77.
(52) Brissot, C.; Rosso, M.; Chazalviel, J.-N.; Lascaud, S. Dendritic Growth Mechanisms in Lithium/Polymer Cells. *J. Power Sources* **1999**, *81-82*, 925−929.
(53) Sadoway, D. R.; Huang, B.; Trapa, P. E.; Soo, P. P.; Bannerjee, P.; Mayes, A. M. Self-Doped Block Copolymer Electrolytes for Solid-State, Rechargeable Lithium Batteries. *J. Power Sources* **2001**, *97-98*, 621−623.
(54) Zhao, C.-Z.; Zhang, X.-Q.; Cheng, X.-B.; Zhang, R.; Xu, R.; Chen, P.-Y.; Peng, H.-J.; Huang, J.-Q.; Zhang, Q. An Anion-Immobilized Composite Electrolyte for Dendrite-Free Lithium Metal Anodes. *Proc. Natl. Acad. Sci. U.S.A.* **2017**, *114*, 11069−11074.
(55) Song, M.; Tan, H.; Chao, D.; Fan, H. J. Recent Advances in Zn-Ion Batteries. *Adv. Funct. Mater.* **2018**, *28*, 1802564.

DOI: 10.1021/acsami.8b14022
ACS Appl. Mater. Interfaces 2018, 10, 38928−38935